Applied Catalysis B: Environmental 100 (2010) 116–123

Contents lists available at ScienceDirect

Applied Catalysis B: Environmental

journal homepage: www.elsevier.com/locate/apcatb

Dechlorination and photodegradation of trichloroethylene by Fe/TiO_2 nanocomposites in the presence of nickel ions under anoxic conditions

Ganesh K. Parshetti, Ruey-an Doong*

Department of Biomedical Engineering and Environmental Sciences, National Tsing-Hua University, 101, Sec. 2, Kuang-Fu Rd., Hsinchu 30013, Taiwan

ARTICLE INFO

Article history:
Received 3 May 2010
Received in revised form 14 July 2010
Accepted 15 July 2010
Available online 22 July 2010

Keywords:
Fe/TiO_2 nanocomposites
Trichloroethylene
Dechlorination
Photodegradation
Nickel ion

ABSTRACT

The removal of priority pollutants by nanocomposites has recently received much attention. In the present study, the dechlorination as well as photodegradation of trichloroethylene (TCE) by the combination of nanoscale zerovalent iron (NZVI) with Degussa P-25 TiO_2 (Fe/TiO_2 nanocomposites) in the presence of nickel ions under anoxic conditions were studied. The Fe/TiO_2 nanocomposites were synthesized by a novel and simple method using polyethylene glycol and sodium borohydride as the cross-linker and reducing agent, respectively. Scanning electron microscopy (SEM) images showed that the NZVI was spherical with the average particle size of 60 ± 5 nm. Electron-probe microanalysis elemental maps showed that the distribution of Fe and Ti in nanocomposites was uniform. The Fe/TiO_2 nanocomposites exhibited excellent ability in dechlorination as well as photodegradation of TCE in the presence of nickel ions. Ethane was found as the major end product of TCE in both dark and photocatalytic reactions, depicting that hydrodechlorination was the major reaction mechanism. In addition, the dechlorination of TCE by Fe/TiO_2 nanocomposites followed the pseudo-first-order kinetics and the rate constant (k_{obs}) for TCE dechlorination was $(1.3 \pm 0.1) \times 10^{-2}\ h^{-1}$, which was higher than that by NZVI alone ($(7.4 \pm 0.2) \times 10^{-3}\ h^{-1}$). The photodegradation efficiency of TCE by Fe/TiO_2 nanocomposites was enhanced in the presence of nickel ions under illumination of UV light at 365 nm. The k_{obs} for TCE photodegradation increased 6.0–11.6 times when Fe/TiO_2 was illuminated with UV light in the presence of nickel ions. A rapid and complete dechlorination of TCE by Fe/TiO_2 nanocomposites was observed after 7 cycles of injection in the presence of nickel ions and UV light, indicating the stability of nanocomposites towards TCE dechlorination.

1. Introduction

Chlorinated hydrocarbons such as tetrachloroethylene and trichloroethylene (TCE) are one of the most prevalent contaminants in the environment, and are released into aquatic environments through the improper treatment and disposal. These chemicals are known to be potentially threatening to the environment and human beings. It is therefore of importance to develop an effective treatment technology to reduce the potential risk of these toxic chemicals in the environment.

The fabrication of nanomaterials for degradation of priority pollutants has recently received considerable attention [1–3]. Zerovalent iron (ZVI) has been successfully employed for the treatment of a large variety of priority pollutants [4–6]. Bimetallic materials including Pd/Fe, Ni/Fe, Cu/Al and Ni/Si have also been found to be effective on reduction of recalcitrant pollutants including chlorinated hydrocarbons [7–10], pentachlorophenol [11] and anions [12]. In addition, the immobilization of nanoparticles onto a support for stabilizing nanoparticles is another strategy to enhance the dechlorination efficiency and rate of chlorinated hydrocarbons under anoxic conditions because of the less agglomeration of nanoparticles and protection of nanoparticles from oxidation [13,14]. Several materials including resin, granule activated carbon, zirconia and membranes have been employed as the supports to avoid the agglomeration of nanoparticles and to accelerate the dechlorination efficiency and rate of chlorinated hydrocarbon [14–17].

Titanium dioxide (TiO_2) is one of the most widely used semiconductors in a wide variety of applications because of its high stability, nontoxicity, high photocatalytic activity, and excellent dielectric properties [18–20]. Several studies have depicted that addition of transition metal ions such as V, Zr, Fe, Ag, Co, and Cu in TiO_2 particles led to an enhanced photoactivity because of the rapid transfer of the photo-generated electrons from the semiconductors to the dopants [21–24]. Addition of iron ions to the sol–gel-derived TiO_2 has been found to enhance the photodegradation efficiency and rate of chlorinated compounds [24]. However, the combination of zerovalent metal with TiO_2 for the degradation

* Corresponding author. Tel.: +886 3 5726785; fax: +886 3 5718649.
E-mail address: radoong@mx.nthu.edu.tw (R.-a. Doong).

0926-3373/$ – see front matter
doi:10.1016/j.apcatb.2010.07.020

of organic compounds has received less attention. Since the nanoscale ZVI (NZVI) has a strong reducing power for reduction of priority pollutants and TiO_2 is an effective photocatalyst, the Fe/TiO_2 nanocomposites can retain both the dechlorination and photocatalytic activity for removal of chlorinated hydrocarbons under anoxic conditions. Huang et al. [25] has depicted that the sol–gel-derived Fe/TiO_2 nanoparticles could enhance the photodegradation efficiency of azo dye under the illumination of UV light. However, the dechlorination ability of Fe/TiO_2 has not been evaluated. In addition, the effect of a catalytic second metal ion on the dechlorination as well as photodegradation of chlorinated hydrocarbons by Fe/TiO_2 nanocomposites remains unclear.

In this study, the combination of NZVI with Degussa P-25 TiO_2 nanoparticles has been prepared for effective removal of TCE under anoxic conditions. A simple reduction method was used to fabricate Fe/TiO_2 nanocomposites by addition of poly(ethylene glycol) (PEG) and sodium borohydride as the cross-linker and reducing agent, respectively. The morphology, structure, elemental distribution, specific surface area and change in chemical species of Fe/TiO_2 nanocomposite were characterized by scanning electron microscopy (SEM), electron-probe microanalysis (EPMA), Brunauer–Emmett–Teller (BET) surface area analyzer and X-ray photoelectron spectroscopy (XPS), respectively. The Fe/TiO_2 nanocomposites were then employed for dechlorination and photocatalytic degradation of TCE under anoxic conditions. In addition, the influence of Ni loading on the removal rates of TCE in the absence and presence of UV light at 365 nm under anoxic conditions was evaluated.

2. Materials and methods

2.1. Chemicals

Trichloroethylene (TCE) (>99.8%, GC grade), N-(2-hydroxyethyl) piperazine-N′-(2-ethanesulfonic acid) (HEPES, $C_8H_{18}N_2SO_4$) and poly(ethylene glycol) (PEG, MW 8400) were purchased from Sigma–Aldrich Co. (Milwaukee, WI). Degussa P-25 TiO_2, a mixture of 80% anatase and 20% rutile, was obtained from Degussa Co. Nickel chloride ($NiCl_2{\cdot}6H_2O$) and ferrous sulfate ($FeSO_4{\cdot}7H_2O$) were obtained from Riedel-de Haën Co. (Seelze, Germany). All other chemicals were of analytical grade and were used as received without further purification. Deoxygenated solutions were prepared with high-purity anoxic deionized water (Millipore, 18.3 MΩ cm) by purging high-purity nitrogen gas (99.995%) in vacuum-sealed bottles. This process was repeated 4–5 times to remove trace amount of oxygen in the solution [26,27].

2.2. Synthesis of Fe/TiO_2 nanocomposite

The PEG-coated TiO_2 was prepared by dissolving 1.19 M PEG into 50 mL of ethanol solution containing 50 mg of Degussa P-25 TiO_2 and stirred for 30 min to form a homogeneous sol of PEG-TiO_2. Nanoscale Fe/TiO_2 nanocomposites were synthesized by adding 50 mL of 1 wt% $FeSO_4{\cdot}7H_2O$ anoxically into the PEG-TiO_2 sol solutions. A faint black color solution of Fe/TiO_2 nanoparticles were obtained by dropwise addition of 0.5 M $NaBH_4$ under constant stirring rate at room temperature. An excess amount of borohydride was used to accelerate the synthetic reaction and then centrifuged at 10,000 × g for 10 min to harvest precipitates. The precipitates were then washed with ethanol and were completely dried under a gentle stream of nitrogen gas to obtain Fe/TiO_2 nanocomposites. The synthesis of pure NZVI nanoparticles was carried out under anoxic conditions by dissolving 0.2 M $FeSO_4{\cdot}7H_2O$ in deionized water at pH 8.0 followed by dropwise addition of 0.5 M $NaBH_4$ to form the black precipitate. The precipitates were then washed with ethanol and dried under N_2 atmosphere.

2.3. Dechlorination of TCE in dark reaction

The dechlorination of 10 μM TCE by Fe/TiO_2 nanocomposites was investigated using 50-mL serum bottles sealed with Teflon-lined rubber septa and aluminum crimp caps. N_2-purged serum bottles were filled with 20 mL of deoxygenated buffer solutions and 0.07 g of Fe/TiO_2 nanoparticles (3.5 g L^{-1}). 10 mM HEPES buffer solution was used to control pH at 7.2 ± 0.1. After being capped with rubber septa and aluminum caps, serum bottles were purged with N_2 immediately to maintain the anoxic conditions. In addition, the deoxygenated stock solutions of Ni(II) ions were delivered into serum bottles by gas-tight syringes to obtain the desired concentrations of 20–100 μM. The bottles were incubated in an orbital shaker at 150 rpm and at 25 ± 1 °C in the dark. Control experiments were also preformed in the absence of Fe/TiO_2 nanocomposites or by NZVI alone. All experiments were carried out in duplicate or triplicate and the average values were reported.

2.4. Photodegradation of TCE

The photocatalytic activity of Fe/TiO_2 nanocomposites towards TCE degradation was conducted by using a batch reactor. High-purity nitrogen gas was purged continuously to maintain anoxic conditions during the preparation of the photodegradation of TCE. A 50-mL serum bottle containing 20 mL of HEPES buffer solution and 10 μM TCE in the presence and absence of Ni(II) was used. An 8 W mercury lamp was positioned within the central part of the photoreactor and cooling water was circulated through a Pyrex jacket surrounding the lamp. After adding Fe/TiO2 nanocomposites to the solution, the sample was sonicated for 20 min under anoxic conditions to obtain a homogeneous dispersion. Immediately after the sonication, the UV light at 365 nm was turned on.

2.5. Analysis of TCE and nonchlorinated hydrocarbons

The headspace analytical technique was used to determine the concentrations of chlorinated and nonchlorinated hydrocarbons. Concentrations of TCE and the byproducts in the headspace of the test bottles were monitored by withdrawing 40 μL of gas in the headspace using a 50-μL gas-tight syringe. The headspace sample was immediately injected into a gas chromatograph (GC) equipped with an electron capture detector (ECD) and a flame ionization detector (FID) (Perkin-Elmer, Autosystem, Norwalk, CT). A 60-m VOCOL fused-silica megabore capillary column (0.545 mm × 3.0 μm, Supelco Co.) was employed to separate the organic compounds. The column was connected to the FID and ECD simultaneously by a Y-splitter; and an optimal sensitivity for chlorinated hydrocarbons was achieved with 40% of the flow (1.85 mL min^{-1}) to the ECD. The column temperature was isothermally maintained at 120 °C using ultra-high-purity nitrogen (>99.9995%) as the carrier and make-up gases. The temperatures of the ECD and FID were maintained at 325 and 250 °C, respectively. The relative standard deviations (RSD) of the ECD analyses were within 10% and those for the FID analyses were within 5%. Control samples were also used to check the possible leakage of target compounds during the incubation process. In addition, concentrations of chlorinated hydrocarbons in aqueous solutions were calculated using the external standard method by preparing the known concentrations of chlorinated hydrocarbons in aqueous solutions.

2.6. Characterization of Fe/TiO_2 nanocomposite

The surface morphology of the Fe/TiO_2 nanocomposites was determined by SEM (JEOL JSM-6700F Oxford Inca Energy 400). All the samples were Pt-coated using Ion Sputter ε-1030 (Hitachi,

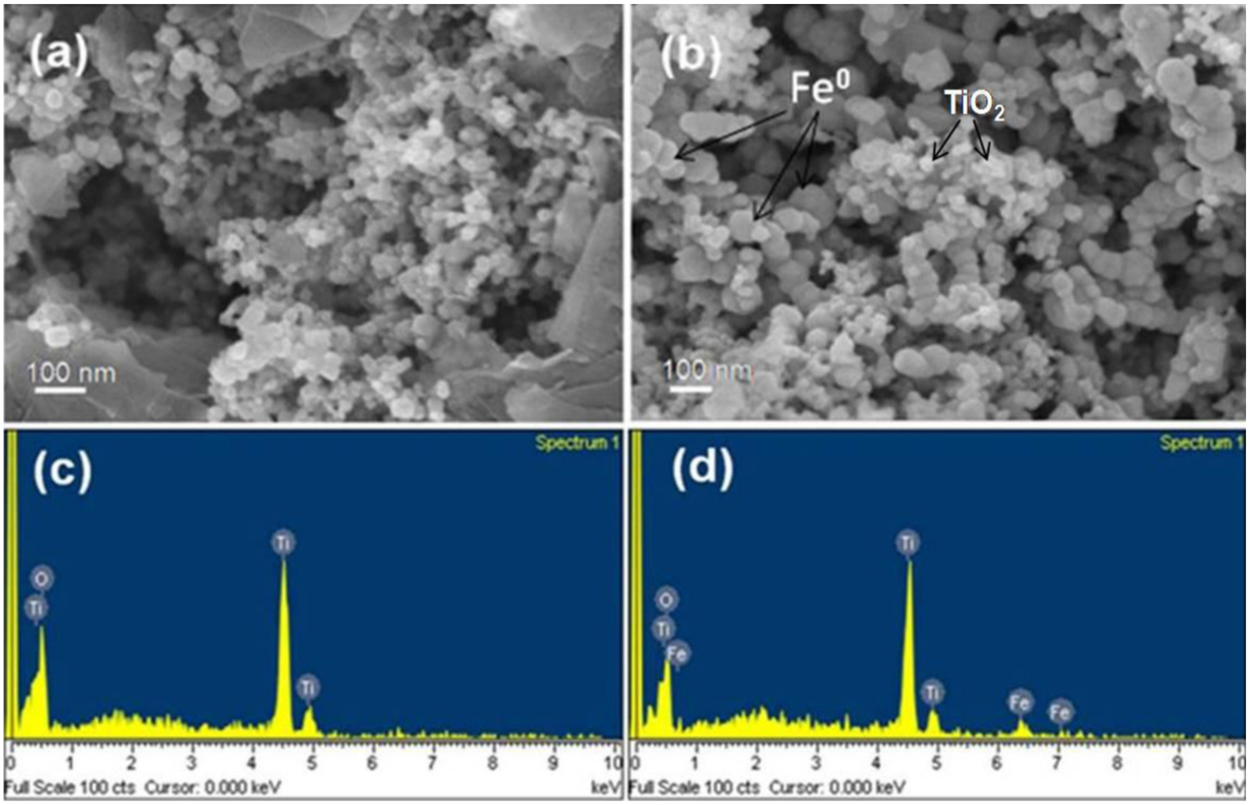

Fig. 1. SEM images of (a) Degussa P-25 TiO_2 and (b) Fe/TiO_2 nanocomposites and EDS spectra of (c) Degussa P-25 TiO_2 and (d) Fe/TiO_2 nanocomposites.

Japan) to increase the conductivity of the sample surface. After coating with Pt, samples were placed under high vacuum (10^{-3}–10^{-7} mbar) conditions. An acceleration electron voltage of 5 kV was applied to obtain the SEM images. EPMA was performed using an electron-probe X-ray microanalyzer (JEOL JXA-8200) with an accelerating voltage of 20 kV and a beam current of 20 nA. Iron and titanium metals were used as the standards for Fe and Ti determination. In addition, Brunauer–Emmett–Teller (BET) surface areas were determined from N_2 adsorption onto the Fe/TiO_2 nanocomposites using Micromeritics ASAP 2020 apparatus. The specific surface areas of Fe/TiO_2, Degussa TiO_2, and NZVI were 60, 48, and 35 $m^2\,g^{-1}$, respectively.

The XPS measurements were performed by an ESCA PHI 1600 photoelectron spectrometer (Physical Electronics, Eden Prairie, MN) using Al Kα X-ray source (1486.6 eV photon energy). The spherical capacitor analyzer with a multi-channel detector had a takeoff angle of 70° related to the horizontal plane of the sample. Data were recorded digitally, and all peak scans were signal averaged until an acceptable signal-to-noise ratio was obtained. During data acquisition, the pressure in the sample chamber maintained below 2.5×10^{-8} Torr. The binding energies of the photoelectrons were determined under the assumption that carbon has a binding energy of 284.8 eV.

The photo-generated free radicals from the photodegradation of TCE by Fe/TiO_2 in the presence of 0–100 μM Ni ion and 5,5-dimethyl-1-pyrroline N-oxide (DMPO) was examined using an electron paramagnetic resonance (EPR) spectrometer (Bruker, EMX-10, Germany) working at X-band frequency of 9.49–9.88 GHz. A 500 W Xe lamp (Ushio Inc.) at major output wavelength of 365 nm was equipped to the sample cavity by lined optical fiber. Nitrogen-purging aqueous Fe/TiO_2 nanocomposites containing TCE, nickel ion and DMPO were irradiated with UV light at room temperature. After illumination for 10 min, the spectra of trapped charges in solutions were recorded at room temperature. The instrumental conditions were set at a center field of 3400–3510 G and a sweep width of 200.0 G.

3. Results and discussion

3.1. Characteristics of Fe/TiO_2 nanocomposites

Fig. 1 shows the SEM images of pristine Degussa P25 TiO_2 nanoparticles and Fe/TiO_2 nanocomposites. The SEM images showed that the particle size distribution of TiO_2 was narrow and the average particle size was 25 ± 5 nm. After the addition of ferrous ion and $NaBH_4$, the NZVI nanoparticles at 60 ± 5 nm were found, and the TiO_2 nanoparticles and NZVI were combined together to form Fe/TiO_2 nanocomposites (Fig. 1b). The EDS analysis from SEM images clearly showed peaks of Ti and Fe in the Fe/TiO_2 nanocomposites (Fig. 1d), and the percentages of iron and titanium in Fe/TiO_2 nanocomposites were 8.0 and 47.1 wt%, respectively.

EPMA was further employed to characterize the distribution patterns of Fe and Ti species in nanocomposites. Fig. 2 shows the EPMA elemental maps of Fe and Ti in TiO_2 and Fe/TiO_2 nanoparticles. For Degussa P-25 TiO_2 nanoparticles, the distribution of Ti was uniform and homogeneous and no Fe was detected. In contrast, both Ti and Fe in Fe/TiO_2 nanocomposites were homogeneously detected with slight agglomeration (Fig. 2c and d). It also reflects the fact that the total amount of TiO_2 on the surface of the nanocomposites was higher than that of Fe, which was in good agreement with the EDS results. In addition, the EPMA results clearly depict that the distribution of Fe and Ti inside Fe/TiO_2 nanocomposites was uniform with little aggregation, which allows good accessibility of the contaminants to Fe/TiO_2 system during dechlorination reaction.

The XPS spectra of Fe/TiO_2 nanocomposites were further examined to understand the change in chemical species (Fig. 3). The O1s spectra show a main peak at 530.6 eV and a shoulder at 532.1 eV.

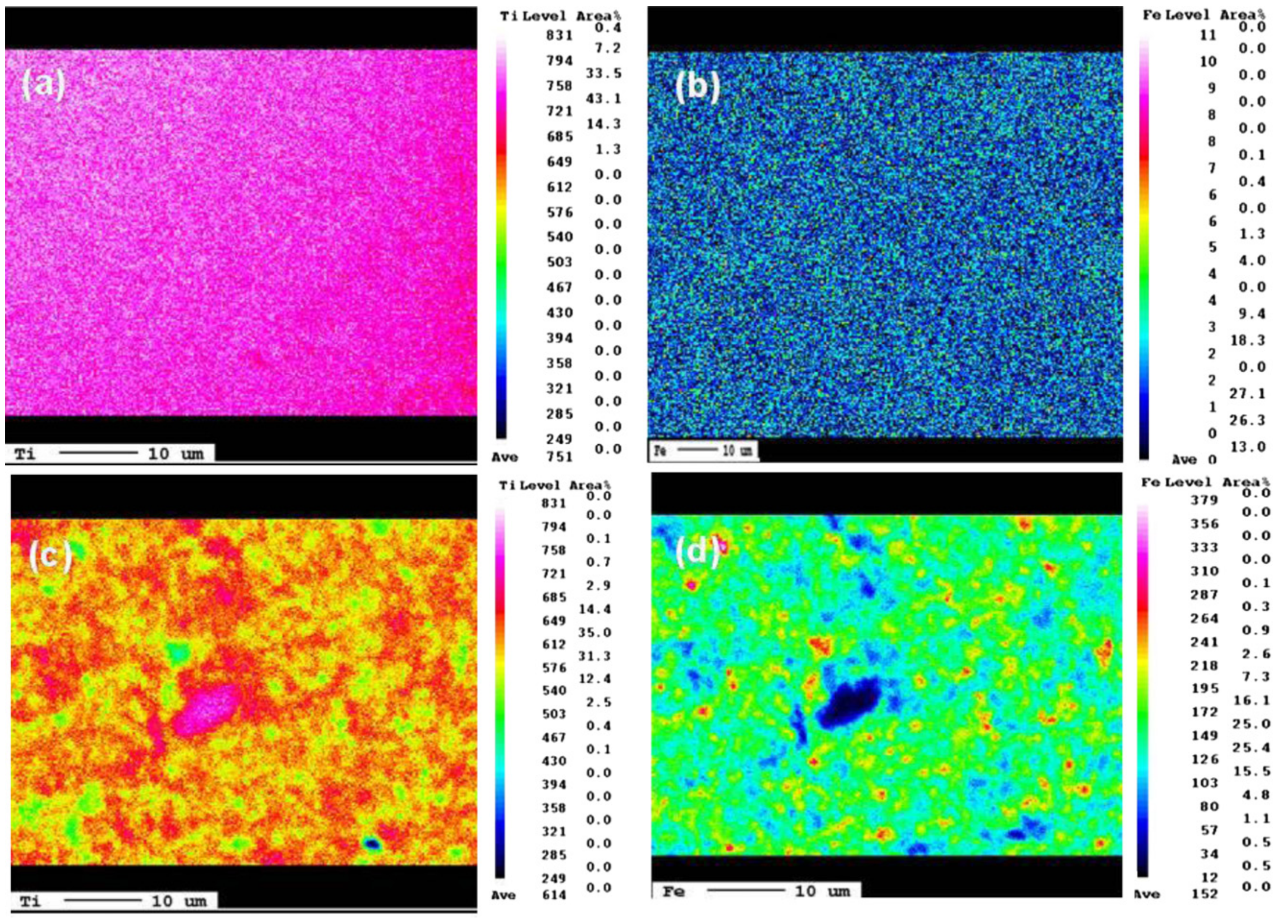

Fig. 2. EPMA images of (a) Ti in Degussa P-25 TiO_2, (b) Fe in Degussa P-25 TiO_2, (c) Ti in Fe/TiO_2 nanocomposites and (d) Fe in Fe/TiO_2 nanocomposites.

The peak at 530.6 eV can be assigned as oxygen bound to tetravalent Ti ions (Ti–O bond) [28]. The Ti2p photoelectron spectra show peaks of $Ti2p_{3/2}$ and $Ti2p_{1/2}$ at 459.1 and 465.0 eV, respectively (Fig. 3b). The doublet separation between the $2p_{1/2}$ and $2p_{3/2}$ peaks was found to be 5.9 eV, which is a characteristic of TiO_2. In addition, two photoelectron peaks at 707 and 720 eV corresponding to the binding energies of $Fe2p_{3/2}$ and $Fe2p_{1/2}$, respectively, were observed (Fig. 3c), which depicts the existence of Fe(0) [29]. It is noteworthy that peaks centered at 711 and 724 eV were observed after deconvolutions of Fe2p peaks (Fig. 3d), clearly indicating the formation of magnetite (Fe_3O_4) onto the surface of NZVI [25,30,31]. The oxide layer is thought to form instantaneously upon NZVI synthesis to passivate the highly reactive Fe(0) core [30]. This disordered nature of the oxide layer supports the phenomenon that the oxide layer allows electron passage through tunneling effects or defect sites, resulting in the preservation of the reducing power of NZVI [30–32].

3.2. Dechlorination of TCE by Fe/TiO_2 nanocomposite under dark condition

The reactivity of Fe/TiO_2 nanocomposites towards TCE dechlorination was examined under anoxic conditions. Fig. 4 shows the dechlorination of 10 μM TCE by different nanoparticles under anoxic conditions. Little TCE was dechlorinated by Degussa P-25 TiO_2 in the dark under anoxic conditions, while 60% of the original TCE was dechlorinated by pure NZVI after the incubation of 150 h. On the contrary, the Fe/TiO_2 nanocomposites exhibited a higher reactivity towards TCE dechlorination than that by NZIL alone, and a removal efficiency of 90% was achieved within 150 h. Ethane was found to be the major product of TCE by Fe/TiO_2 and the carbon mass balance was up to 90% (Fig. 4b), indicating that hydrodechlorination is the major reaction mechanism for TCE dechlorination by Fe/TiO_2 nanocomposites.

The TCE degradation can be described by pseudo-first-order rate equation [33,34]:

$$\frac{dC_{\mathrm{TCE}}}{dt} = -k_{\mathrm{obs}} C_{\mathrm{TCE}} \quad (1)$$

where k_{obs} is the pseudo-first-order rate constant (h^{-1}), t is reaction time (h), and C_{TCE} is the aqueous concentration of TCE (μM). The k_{obs} for TCE dechlorination by NZVI and Fe/TiO_2 nanoparticles was $(7.4 \pm 0.2) \times 10^{-3}$ and $(1.3 \pm 0.1) \times 10^{-2}\ h^{-1}$, respectively. The increase in rate constant for TCE dechlorination by Fe/TiO_2 may be attributed to the uniform dispersion of zerovalent iron in nanocomposites, resulting in the increase in active sites for dechlorination. This is also the first report on the enhanced dechlorination of chlorinated compounds by Fe/TiO_2 nanocomposites not involving photolysis.

3.3. Effect of Ni(II) ion TCE dechlorination under dark conditions

Although Fe/TiO_2 is effective on the removal of TCE under anoxic conditions, the reactivity of the nanocomposites is highly controlled by the surface characteristics and nature of contaminants. The deposition of small amounts of second catalytic metal ion such as Ni and Pd onto the zerovalent metal surface has been demonstrated to enhance the dechlorination efficiency and rate of chlorinated hydrocarbons [35–37]. In this study, various concentrations of Ni(II) ranging from 20 to 100 μM (1.2–5.8 mg L^{-1}) were amended into the Fe/TiO_2 nanocomposites to understand the syn-

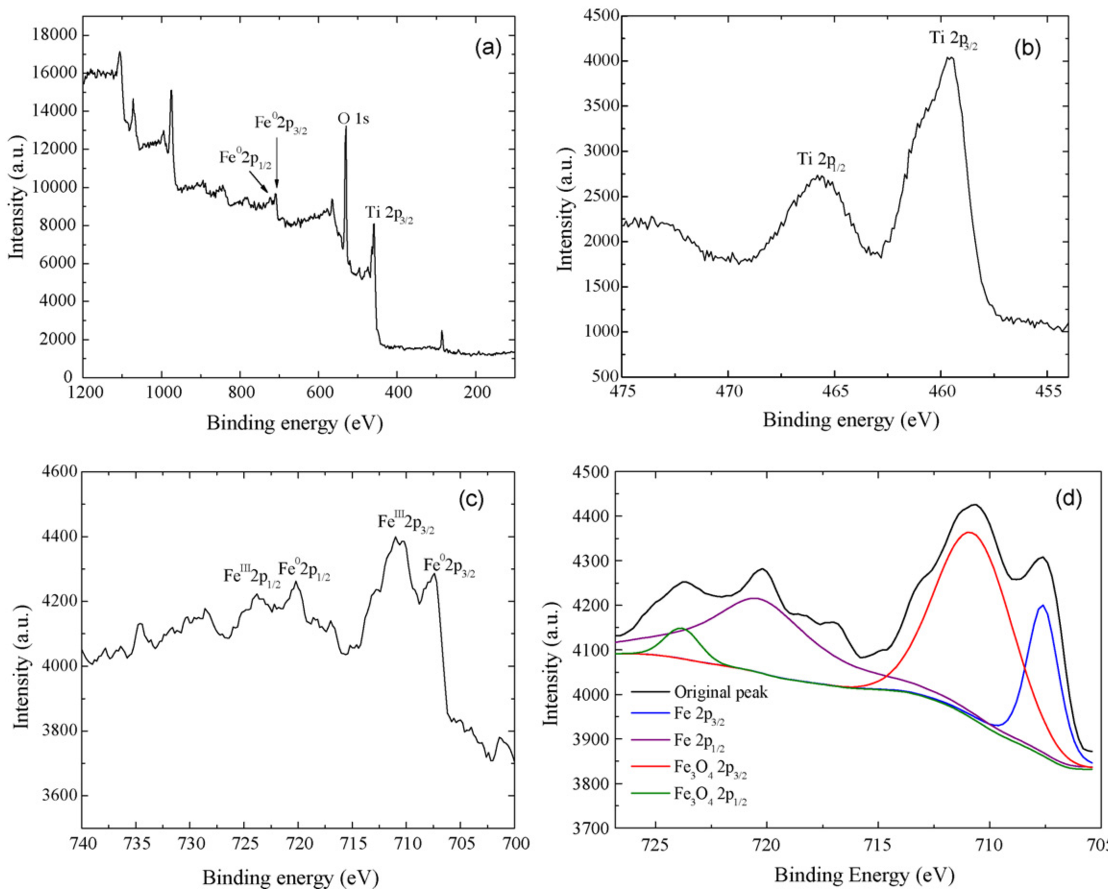

Fig. 3. X-ray photoelectron (XPS) spectra of (a) full survey, (b) Ti2p, and (c) Fe2p of Fe/TiO_2 nanocomposites. (d) The peak deconvolution of Fe 2p peak.

ergistic effect of second catalytic metal ion on dechlorination and photodegradation efficiencies of TCE by Fe/TiO_2 nanocomposites. Fig. 5 shows the dechlorination rate of TCE by Fe/TiO_2 as a function of Ni(II) concentration in the dark under anoxic conditions. Addition of Ni(II) has a significant effect on the enhancement of TCE dechlorination, and the dechlorination efficiency and rate of TCE increased upon increasing Ni(II) concentrations. The k_{obs} for TCE dechlorination by Fe/TiO_2 increased from $0.13 \pm 0.02\,h^{-1}$ at 20 μM ($r^2 = 0.91$) to $1.29 \pm 0.06\,h^{-1}$ at 100 μM ($r^2 = 0.97$). These values are, in general, 1–2 orders of magnitude higher than that in the absence of Ni(II), clearly depicting that addition of Ni(II) has a synergistic effect on the dechlorination of TCE by Fe/TiO_2 nanocomposites. The increase in k_{obs} for TCE dechlorination may be attributed to the high catalytic ability of Ni onto Fe/TiO_2 nanocomposites in dehydrogenation reaction in the presence of nickel ion. In this study, the Ni(II) concentrations in aqueous solutions after the reactions were determined to be 0.075–0.184 mg L^{-1} when 20–100 μM Ni(II) were added, showing that 94–97% of Ni(II) were adsorbed onto the surface of Fe/TiO_2 nanocomposites. These adsorbed nickel ions would partially reduce to its zerovalent species to form bimetallic Fe/Ni nanoparticles [27,34]. In bimetallic Ni/Fe systems, iron acts as the reductant for water and Ni serves as a catalyst to prevent the formation of toxic byproducts by hydrodechlorination of chlorinated compounds via hydrogen reduction rather than via electron transfer [38,39].

3.4. Photo-enhanced dechlorination of TCE by Fe/TiO_2 in the presence of Ni(II)

One of the advantages of Fe/TiO_2 nanocomposites is the photocatalytic activity towards organic degradation. In this study, the photocatalytic activity of Degussa P-25 TiO_2 and Fe/TiO_2 nanoparticles towards TCE dechlorination in the absence and presence of Ni(II) ions was further evaluated. As depicted in Fig. 6, no obvious photodegradation of TCE was observed within 60 min in the presence of Degussa P-25 TiO_2, NZVI, or Fe/TiO_2 nanocomposites under anoxic conditions. Addition of 100 μM Ni(II) to solutions containing NZVI or Degussa P-25 TiO_2 alone also had little effect on the enhancement of dechlorination efficiency of TCE within 60 min of UV irradiation. In contrast, the photodegradation efficiency of TCE was significantly enhanced when Ni(II) was added into the solution containing Fe/TiO_2 nanocomposites. 65% of the original TCE was dechlorinated within 60 min when 20 μM Ni(II) was added in the presence of UV light. The photodegradation efficiency of TCE increased upon increasing Ni(II) concentration, and a nearly complete dechlorination of TCE by Fe/TiO_2 nanocomposites was observed when Ni(II) concentrations were higher than 50 μM, clearly depicting that addition of Ni(II) ions has a prominent effect on photo-enhanced dechlorination of TCE under anoxic conditions. Similar to the dechlorination of TCE by Fe/TiO_2 in the dark reaction, ethane was found to be the major product of TCE photo-dechlorination by Fe/TiO_2 in the presence of Ni(II) ions with carbon mass balance of 94%. This result clearly demonstrates that hydrodechlorination is the major reaction pathway of TCE by Fe/TiO_2 in the presence of Ni(II) under illumination of 365 nm UV light (Fig. 6b).

The photo-enhanced dechlorination of TCE by Fe/TO_2 also followed the pseudo-first order kinetics and the k_{obs} for TCE photo-dechlorination increased significantly from $0.98 \pm 0.01\,h^{-1}$ at 20 μM Ni(II) to $14.91 \pm 0.78\,h^{-1}$ at 100 μM Ni(II). These values are 6.0–11.6 times higher than those in the absence of UV light (Fig. 7). The increase in k_{obs} for TCE dechlorination may be due primarily to

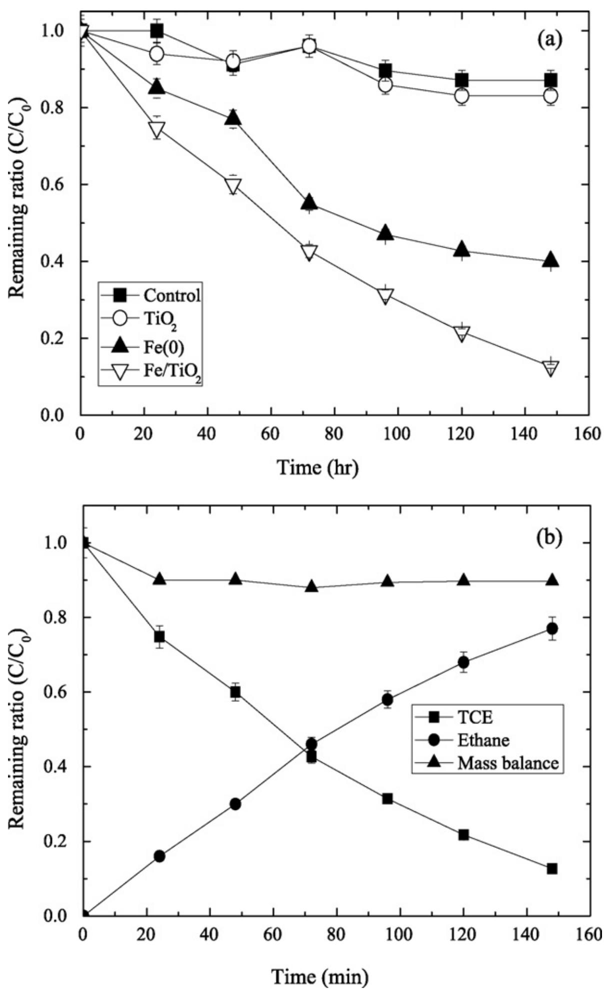

Fig. 4. (a) Dechlorination of TCE by different nanomaterials under anoxic conditions and (b) carbon mass balance of TCE dechlorination by Fe/TiO_2 nanocomposites. The concentrations of TCE and nanoparticles were 10 μM and 3.5 g L^{-1}, respectively.

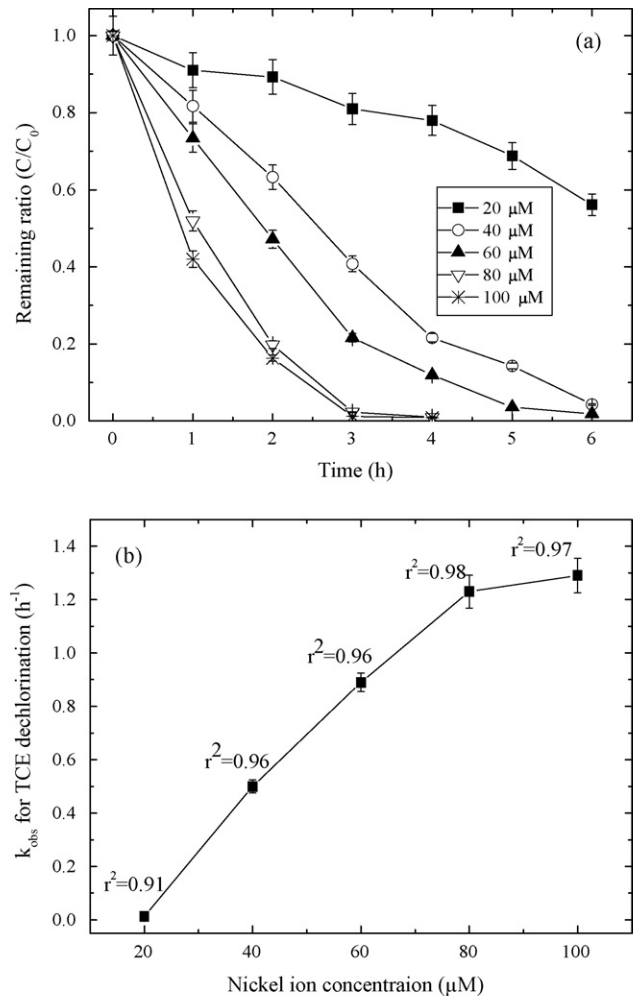

Fig. 5. Effect of nickel ion on TCE dechlorination by Fe/TiO_2 nanocomposites under anoxic conditions. (a) Dechlorination of TCE by Fe/TiO_2 at various concentrations of nickel ion and (b) the k_{obs} for TCE dechlorination as a function of nickel ion concentration.

the generation of radicals, resulting in enhancing the electron transfer efficiency for TCE dechlorination. Fig. 8 shows the change in the intensity of EPR signals of free radicals produced from the irradiation of aqueous TCE solution containing Fe/TiO_2 nanocomposites in the presence of DMPO and various concentrations of nickel ions. Addition of DMPO produced six-line EPR spectra after 10 min of UV light irradiation, revealing the formation of O-centered radical adducts such as $^{\bullet}OH$, $^{\bullet}OOH$, and $ROO^{\bullet}$ [40,41]. The EPR signal of the radical spin adducts was very weak when no nickel ion was added to the photoreaction of TCE by Fe/TiO_2 nanocomposites. However, the signal intensity of free radicals increased obviously upon increasing aqueous nickel ion concentrations from 20 to 100 μM (Fig. 8a), which clearly indicates the enhanced effect of nickel ions on the production of radicals. In addition, the EPR spectrum of nickel ion after UV irradiation showed two marked spin signals at two different sites, $g = 2.000$ and 2.4856 (Fig. 8b), presumably due to the formation of Ni^{3+} ion when Ni^{2+} was added to the Fe/TiO_2 nanocomposites during photodegradation of TCE [42]. This means that Ni^{2+} ions could behave as the hole trap to oxidize to Ni^{3+} ions under anoxic conditions, and the formed Ni^{3+} ions could further react with hydroxyl anions or trap the photo-generated electrons to reduce to Ni^{2+} ions again [43]. Therefore, the photo-generated electron–hole pairs can thus be separated through Ni ion cycling, leading to the improvement of electron transfer efficiency and rapid dechlorination rate of TCE by Fe/TiO_2:

$$Ni^{3+} + OH^- \rightarrow Ni^{2+} + {}^{\bullet}OH \tag{2}$$

$$Ni^{3+} + e^- \rightarrow Ni^{2+} \tag{3}$$

In addition, the turnover number of this photocatalytic reaction, defined as the mole of TCE that Fe/TiO_2 nanocomposites can covert, was calculated to be 0.1, which clearly shows that the dechlorination is a photo-assisted reaction [44].

3.5. Effect of pH on dechlorination of TCE by Fe/TiO_2

Fig. 9 shows the pseudo-first-order rate constants for TCE dechlorination by Fe/TiO_2 as a function of pH under dark and UV-irradiation conditions. The k_{obs} for TCE dechlorination decreased rapidly from $0.30 \pm 0.013\ h^{-1}$ at pH 2 to $0.03 \pm 0.002\ h^{-1}$ at pH 6 and then changed slightly when pH was higher than 7.0 under dark conditions. In the presence of 100 μM Ni(II) and UV light, the k_{obs} for TCE dechlorination were in the range (13.1 ± 0.7)–$15.4 \pm 0.8\ h^{-1}$ at pH lower than 7 and then decreased dramatically under alkaline conditions. These results clearly indicate that the pH value has a great effect on the removal efficiency of TCE by Fe/TiO_2 and the dechlorination efficiency and rate of TCE decreased significantly under alkaline conditions. The growth of iron oxides onto the reactive surface sites of NZVI during dechlorination processes is one

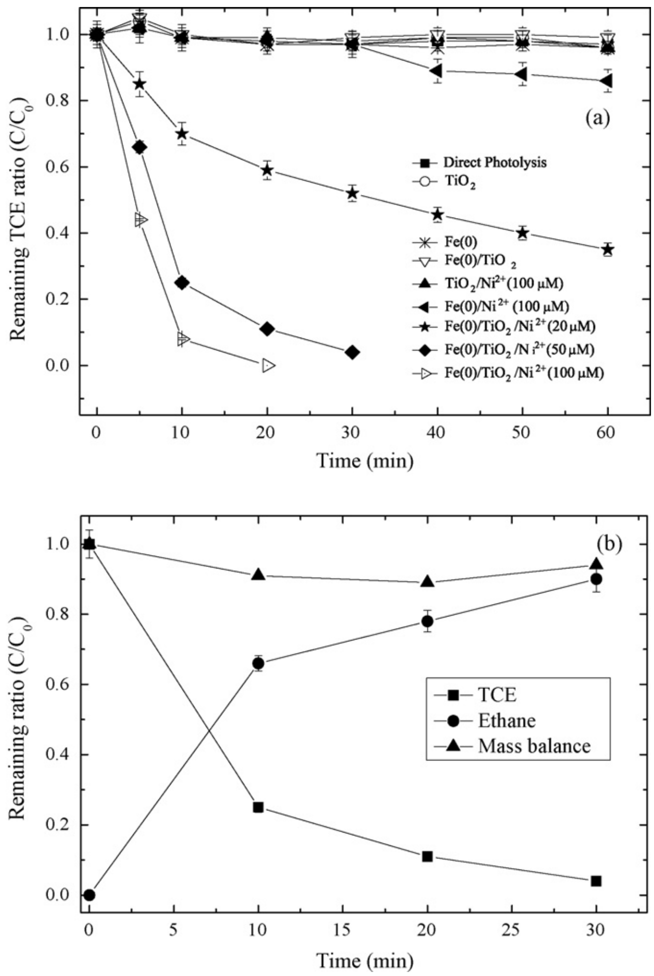

Fig. 6. (a) Photodegradation of TCE by different nanoparticles under anoxic conditions in the presence and absence of nickel ions and (b) carbon mass balance of TCE photodegradation by Fe/TiO_2 nanocomposites at 50 μM Ni(II). The concentrations of TCE and nanoparticles were 10 μM and 3.5 g L^{-1}, respectively. The wavelength of UV light was 365 nm.

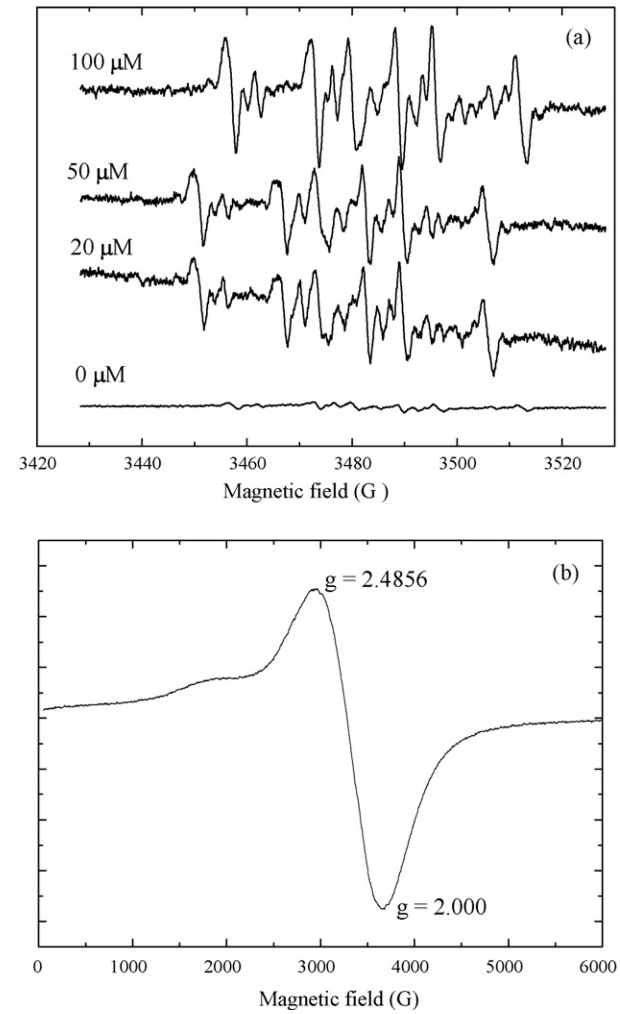

Fig. 8. The EPR signals of (a) radicals produced from the irradiation of TCE-containing aqueous Fe/TiO_2 nanocomposites in the presence of DMPO and various concentrations of nickel ions and (b) nickel ion during the photodegradation of TCE by Fe/TiO_2 nanocomposites.

of the plausible reasons for the decrease in reactivity of Fe/TiO_2. Several studies have depicted that the prolonged exposure to the aqueous solutions resulted in the growth of hydroxylated iron oxide films that deactivated the Fe surface [5,34]. The dechlorination of chlorinated hydrocarbons by ZVI is a surface-mediated reaction that is largely controlled by the available surface sites. The reaction of zerovalent iron with water produced Fe^{2+} and OH^-, and then to form ferrous hydroxide ($Fe(OH)_2$). The ferrous hydroxide would further transform to ferric oxides under alkaline conditions.

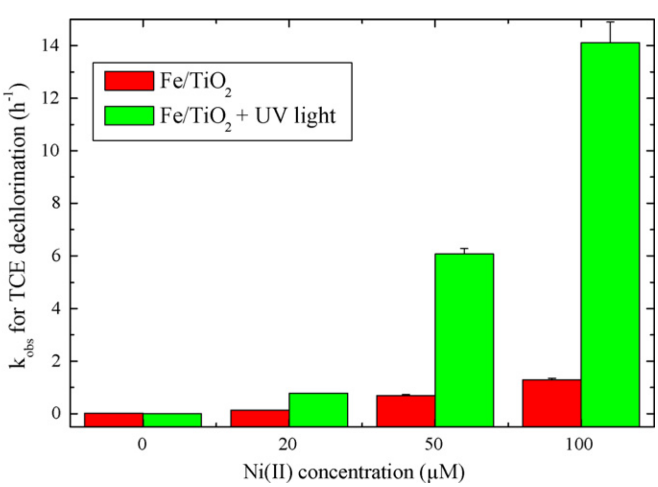

Fig. 7. Comparison of the k_{obs} for TCE dechlorination by Fe/TiO_2 nanocomposites in the dark and photo-enhanced reactions at various Ni(II) concentrations.

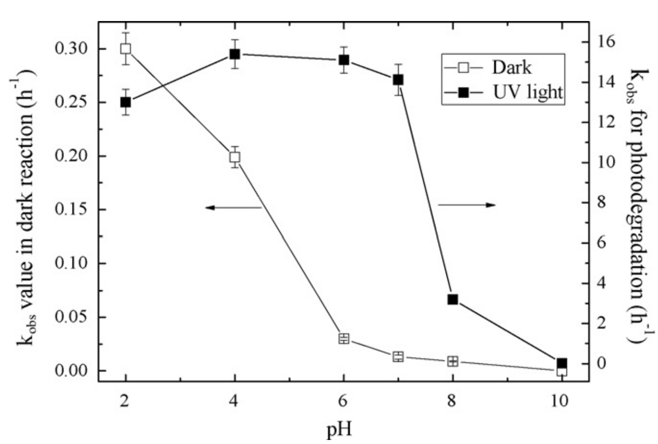

Fig. 9. The pseudo-first-order rate constant (k_{obs}) for TCE dechlorination by Fe/TiO_2 nanocomposites as a function of pH ranging from 2 to 10 under dark and photo-enhanced conditions.

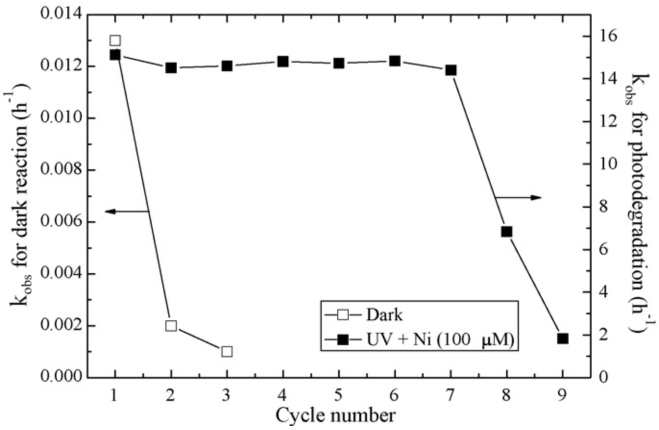

Fig. 10. Stability and durability of Fe/TiO_2 nanocomposites in TCE dechlorination under dark and photo-enhanced conditions.

In addition, the surface passivation layers would be formed at high pH value due to the precipitation of ferric hydroxide and metal carbonates, resulting in low dechlorination efficiency of TCE by Fe/TiO_2 at high pH values.

3.6. Stability and durability of Fe/TiO_2 nanocomposites

The stability and possible long-term performance of Fe/TiO_2 nanocomposites on the dechlorination of TCE were evaluated by repeatedly injection of 10 μM TCE solutions into the 20 mL solutions at pH 7 under dark and UV-irradiation conditions. As depicted in Fig. 10, the reduction capacity of Fe/TiO_2 nanocomposites towards TCE dechlorination decreased significantly under dark conditions. On the other hand, the photo-reduction capacity of the Fe/TiO_2 nanocomposites in the presence of 100 μM Ni(II) ions under UV-irradiation conditions could be maintained for 7 spikes. Further addition of the TCE concentration decreased the dechlorination efficiency and rate of TCE, presumably due to the accumulation of iron oxides on the surface of Fe/TiO_2. However, the k_{obs} for TCE dechlorination under UV-irradiation conditions was still higher than those in dark reaction, clearly indicating that the Fe/TiO_2 nanocomposites can serve as an environmentally friendly material for the enhanced dechlorination of chlorinated hydrocarbons for long-term performance under UV-irradiation conditions.

4. Conclusions

In this study, we have first demonstrated the rapid dechlorination and photodegradation of TCE by Fe/TiO_2 nanocomposites in the presence of nickel ions and UV light under anoxic conditions. The nanoscale Fe/TiO_2 was synthesized by one-pot simple reduction method for dechlorination of TCE in the presence of nickel ions. Surface analyses indicated that the NZVI and TiO_2 were homogeneously dispersed in the nanocomposites with little aggregation. The Fe/TiO_2 nanocomposites showed excellent ability towards TCE dechlorination in the presence of nickel ions. The presence of nickel ions in the concentration range 20–100 μM significantly enhanced the dechlorination of TCE both in dark and photo-induced reactions. Ethane was found to be the major end product of TCE dechlorination in both dark and photo-enhanced reactions, depicting that hydrodechlorination is the main mechanism. The pH value has a great effect on the removal efficiency of TCE by Fe/TiO_2 and the dechlorination efficiency and rate of TCE decreased obviously under alkaline conditions. In addition, the Fe/TiO_2 nanocomposites can retain the high photocatalytic reactivity after 7 cycles of injection in the presence of nickel ion and 365 nm UV light. Results obtained in this study clearly indicate that the Fe/TiO_2 nanocomposites synthesized by a simple route can be useful nanomaterials for removal of various chlorinated compounds by dechlorination as well as by photocatalytic degradation.

Acknowledgment

The authors thank the National Science Council, Taiwan for financial support under contract no. NSC-98-2221-E-007-030-MY3.

References

[1] W.C. Hung, S.H. Fu, J.J. Tseng, H. Chu, T.H. Ko, Chemosphere 66 (2007) 2142–2151.
[2] W.X. Zhang, J. Nanoparticle Res. 5 (2003) 323–332.
[3] T. Phenrat, Y.Q. Liu, R.D. Tilton, G.V. Lowry, Environ. Sci. Technol. 43 (2009) 1507–1514.
[4] A.B.M. Giasuddin, S.R. Kanel, H. Choi, Environ. Sci. Technol. 41 (2007) 2022–2027.
[5] M.O. Nutt, J.B. Hughes, M.S. Wong, Environ. Sci. Technol. 39 (2005) 1346–1353.
[6] C.L. Hsueh, Y.H. Huang, C.Y. Chen, J. Hazard. Mater. 129 (2006) 228–233.
[7] F. He, D.Y. Zhao, Appl. Catal. B: Environ. 84 (2008) 533–540.
[8] Y.H. Tee, E. Grulke, D. Bhattacharyya, Ind. Eng. Chem. Res. 44 (2005) 7062–7070.
[9] D.M. Cwiertny, S.J. Bransfield, K.J.T. Livi, D.H. Fairbrother, A.L. Roberts, Environ. Sci. Technol. 40 (2006) 6837–6843.
[10] J. Feng, T.T. Lim, Chemosphere 59 (2005) 1267–1277.
[11] U.D. Patel, S. Suresh, J. Hazard. Mater. 156 (2008) 308–316.
[12] L. Xie, C. Shang, Chemosphere 64 (2006) 919–930.
[13] J. Xu, D. Bhattacharya, Environ. Prog. 24 (2005) 358–366.
[14] G.K. Parshetti, R.A. Doong, Water Res. 43 (2009) 3086–3094.
[15] C.J. Lin, S.L. Lo, Y.H. Kiou, Chemosphere 59 (2005) 1299–1307.
[16] J.G. Darab, A.B. Amonette, D.S.D. Burke, R.D. Orr, S.M. Ponder, B. Schrick, T.E. Mallouk, W.W. Lukens, D.L. Caulder, D.K. Shuh, Chem. Mater. 19 (2007) 5703–5713.
[17] H. Choi, S.R. Al-Abed, S. Agarwal, D.D. Dionysiou, Chem. Mater. 20 (2008) 3649–3655.
[18] M.A. Barakat, Y.T. Chen, C.P. Huang, Appl. Catal. B: Environ. 53 (2004) 13–20.
[19] K. Nagaveni, M.S. Hegde, G. Madras, J. Phys. Chem. B 108 (2004) 20204–20212.
[20] H. Zhang, G. Chen, Environ. Sci. Technol. 43 (2009) 2905–2910.
[21] J. Zhu, W. Zheng, B. He, J. Zhang, M. Anpo, J. Mol. Catal. A: Chem. 216 (2004) 35–43.
[22] J.C. Colmenares, M.A. Aramendía, A. Marinas, J.M. Marinas, F.J. Urbano, Appl. Catal. A: Gen. 306 (2006) 120–127.
[23] S.M. Chang, C.Y. Hou, P.H. Lo, C.T. Chang, Appl. Catal. B: Environ. 90 (2009) 233–241.
[24] W.C. Hung, Y.C. Chen, H. Chu, T.K. Tseng, Appl. Surf. Sci. 255 (2008) 2205–2213.
[25] C.P. Huang, W.P. Hsieh, J.R. Pan, S.M. Chang, Sep. Purif. Technol. 58 (2007) 152–158.
[26] R.A. Maithreepala, R.A. Doong, Environ. Sci. Technol. 38 (2004) 260–268.
[27] R.A. Doong, Y.L. Lai, Chemosphere 64 (2006) 371–378.
[28] A. Sandell, M.P. Andersson, M.K.J. Johansson, P.G. Karlsson, Y. Alfredsson, J. Schadt, H. Siegbahn, P. Uvdal, Surf. Sci. 530 (2003) 63–70.
[29] R.A. Doong, K.T. Chen, H.C. Tsai, Environ. Sci. Technol. 37 (2003) 2575–2581.
[30] J.T. Nurmi, P.G. Tratnyek, V. Sarathy, D.R. Baer, J.E. Amonette, K. Pecher, C.M. Wang, J.C. Linehan, D.W. Matson, R.L. Penn, M.D. Driessen, Environ. Sci. Technol. 39 (2005) 1221–1230.
[31] M.A.V. Ramos, W. Yan, X.Q. Li, B.E. Koel, W.X. Zhang, J. Phys. Chem. C 113 (2009) 14591–14594.
[32] X.Q. Li, W.X. Zhang, Langmuir 22 (2006) 4638–4642.
[33] C.J. Clark II, P.S.C. Rao, M.D. Annable, J. Hazard. Mater. B 96 (2003) 65–78.
[34] R.A. Doong, Y.L. Lai, Water Res. 39 (2005) 2309–2318.
[35] B. Schrick, J.L. Blough, A.D. Jones, T.E. Mallouk, Chem. Mater. 14 (2002) 5140–5147.
[36] C.C. Lee, R.A. Doong, Environ. Sci. Technol. 42 (2008) 4752–4757.
[37] Y.H. Tee, L. Bachas, D. Bhattacharyya, J. Phys. Chem. C 113 (2009) 9454–9464.
[38] T. Li, J. Farrell, Environ. Sci. Technol. 35 (2001) 3560–3565.
[39] B. Schrick, B.W. Hydutsky, J.L. Blough, T.E. Mallouk, Chem. Mater. 16 (2004) 2187–2193.
[40] V. Brezova, D. Dvoranova, A. Stasko, Res. Chem. Intermed. 33 (2007) 251–268.
[41] S.I. Dikalov, R.P. Mason, Free Radic. Biol. Med. 27 (1999) 864–872.
[42] T.K. Ghorai, D. Dhak, S. Dalai, P. Pramanik, J. Alloys Compd. 463 (2008) 390–397.
[43] L.G. Devi, N. Kottam, N.S.G. Kumar, K.E. Raiashekhar, Cent. Eur. J. Chem. 8 (2010) 142–148.
[44] N. Serpone, A. Salinaro, A. Emeline, V. Ryabchuk, J. Photochem. Photobiol. A: Chem. 130 (2000) 83–94.